

# ADVANCED LLRF SYSTEM SETUP TOOL FOR RF FIELD REGULATION OF SRF CAVITIES

S. Pfeiffer\*, J. Branlard, M. Hoffmann, C. Schmidt  
DESY, Hamburg, Germany

## Abstract

Feedback operation at the European XFEL ensures an amplitude and phase stability of 0.01% and 0.01 deg, respectively. To reach such high RF field stability, model-based approaches for RF field system characterization and RF field controller design are in use. High demand on this system modelling is set especially to the characterization of additional passband modes for small bandwidth SRF cavities operated in pulsed mode and vector-sum regulation. This contribution discusses the developed "ADVANCED SYSTEM SETUP TOOL" using a graphical user implementation in MATLAB® for the RF field system characterization and the multiple-input-multiple-output feedback controller setup. Examples and current limitations will be presented.

## INTRODUCTION

The free-electron laser FLASH and the European XFEL operate superconducting radio frequency (SRF) cavities; high quality resonators studied at DESY. They are operated at a frequency of 1.3 GHz with field gradients beyond 30 MV/m. In order to achieve precise FEL timing stability and reliable machine operation it is required to control the electro-magnetic fields inside the cavities with extremely high precision. The root mean square (RMS) values of the error between the setpoint and field gradient are requested to be lower than 0.01% in amplitude and 0.01° in phase [1]. The RF field regulation is done by measuring the stored electro-magnetic field inside the cavities and processing this information by the feedback controller to modulate the driving RF source. The digital electronic standard in which the low-level radio frequency (LLRF) systems are realized is Micro Telecommunications Computing Architecture (MicroTCA.4) [2]. It was experimentally verified that a control scheme consisting of an iterative learning feedforward component and a linear multiple input multiple output (MIMO) feedback controller is able to cope with these requirements, [3–7]. The design of the feedback controller and learning feedforward relies on a linear system model identified from special series of measurements.

The identification and advanced system setup started at FLASH with individual MATLAB® scripts. These scripts were further developed and extended for various facilities over the years. The goal of combining all scripts into one tool, see Fig. 1, is to keep it up to date for all facilities without changing each tool separately. The paper gives a short introduction into the developed graphical MATLAB® based "ADVANCED SYSTEM SETUP TOOL".

\* sven.pfeiffer@desy.de

## PROBLEM DESCRIPTION

The systematic setup of advanced regulation concepts is often a task for an experienced system engineer. Such advanced setup schemes requires basic system theoretical background and deeper knowledge of the plant to be regulated, the system modelling, feedback controller design, stability analysis for systems operated in closed feedback loop, design of iterative learning schemes, system latency constraints, usable numerical values and its fixed point constraints within FPGA and others. This "ADVANCED SYSTEM SETUP TOOL" supports the system expert by centralizing the necessary information and providing exception handling.

### Cavity White Box Model

The dynamical system behavior is modelled by using the physical cavity equation from [8]. The latter is well known in accelerator physics and can be described by the differential equation

$$\frac{d}{dt} \begin{bmatrix} V_I(t) \\ V_Q(t) \end{bmatrix} = \begin{bmatrix} -\omega_{1/2} & -\Delta\omega \\ \Delta\omega & -\omega_{1/2} \end{bmatrix} \begin{bmatrix} V_I(t) \\ V_Q(t) \end{bmatrix} + R_L \omega_{1/2} \begin{bmatrix} I_I(t) \\ I_Q(t) \end{bmatrix}, \quad (1)$$

in which  $V(t)$  is the complex cavity voltage,  $I(t)$  the complex driving current,  $\omega_{1/2}$  as half-bandwidth,  $\Delta\omega = \omega_0 - \omega$  the detuning and  $R_L$  the shunt impedance of the cavity. Hereby the subscript  $I$  and  $Q$  denotes the in-phase and quadrature component, respectively.

Redefining the output vector  $V(t)$  as  $y(t)$  and the input vector  $R_L I(t)$  as  $u(t)$  leads to the state space representation of

$$\begin{bmatrix} \dot{y}_I \\ \dot{y}_Q \end{bmatrix} = \overbrace{\begin{bmatrix} -\omega_{1/2} & -\Delta\omega \\ \Delta\omega & -\omega_{1/2} \end{bmatrix}}^A \begin{bmatrix} y_I \\ y_Q \end{bmatrix} + \overbrace{\begin{bmatrix} \omega_{1/2} & 0 \\ 0 & \omega_{1/2} \end{bmatrix}}^B \begin{bmatrix} u_I \\ u_Q \end{bmatrix}, \quad (2)$$

$$\begin{bmatrix} y_I \\ y_Q \end{bmatrix} = \underbrace{\begin{bmatrix} 1 & 0 \\ 0 & 1 \end{bmatrix}}_C \begin{bmatrix} y_I \\ y_Q \end{bmatrix},$$

with system matrix  $A$ , input matrix  $B$  and output matrix  $C$ . The transformation of (2) into the Laplace domain by

$$\frac{Y(s)}{U(s)} = G(s) = C(s \cdot I - A)^{-1} B \quad (3)$$

gives the MIMO transfer function

$$G(s) = \frac{(\omega_{1/2})}{(\Delta\omega)^2 + (s + \omega_{1/2})^2} \begin{bmatrix} s + (\omega_{1/2}) & -\Delta\omega \\ \Delta\omega & s + (\omega_{1/2}) \end{bmatrix}. \quad (4)$$

Content from this work may be used under the terms of the CC BY 3.0 licence (© 2019). Any distribution of this work must maintain attribution to the author(s), title of the work, publisher, and DOI.

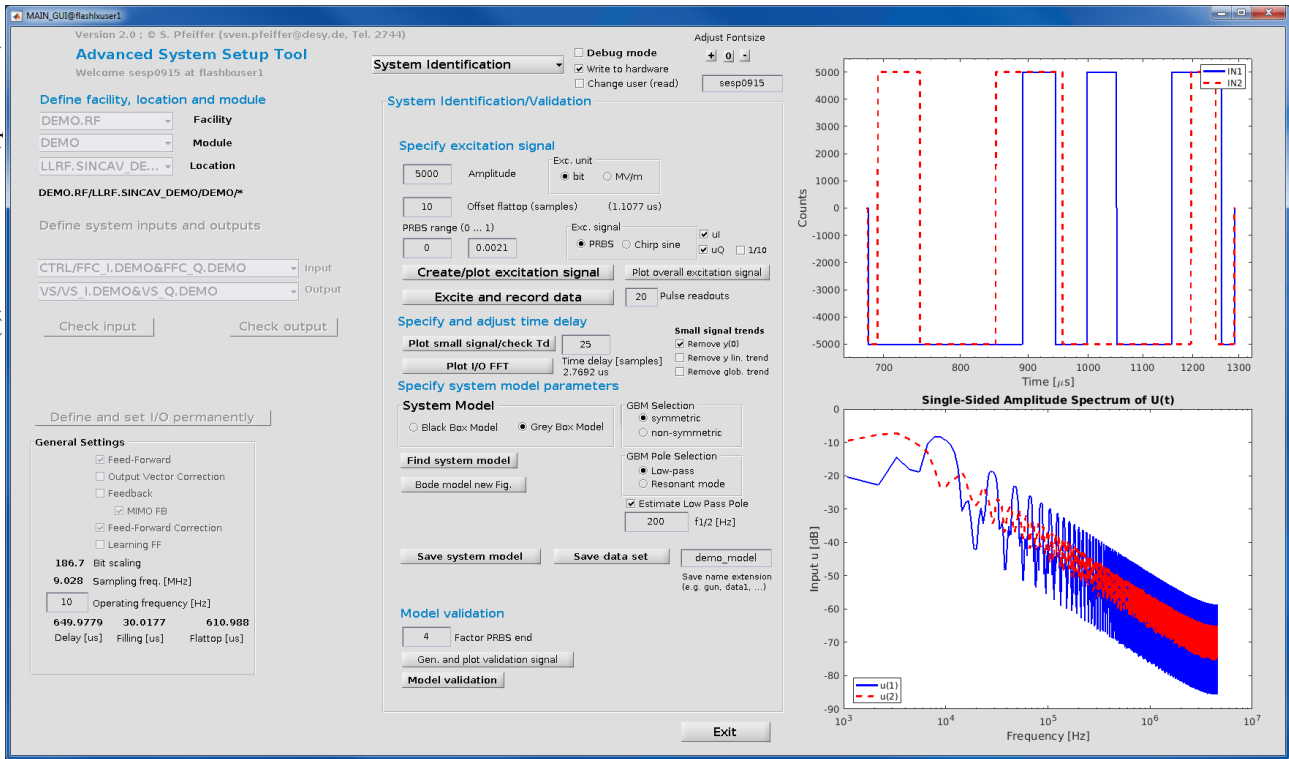


Figure 1: Overview of the tool with system identification as chosen method.

The cavity equation is developed around the baseband frequency, meaning the fundamental  $\pi$ -mode is located at frequency zero. This differential equation holds only for a single mode in frequency, e.g. the  $\pi$ -mode. In total nine modes need to be considered for 9-cell TESLA type SRF cavity. The complete cavity baseband model can be obtained by the superposition of all nine modes

$$G_{Cav}(s) = \sum_{n=1}^9 G_{\frac{n}{9}\pi}(s). \quad (5)$$

The derivation of passband modes with their characteristics is shown in [9]. The half-bandwidth  $\omega_{1/2} = \omega_0/(2Q_L)$  of the additional passband modes is in the order of the fundamental  $\pi$ -mode, see Table 1. Figure 2 shows the resulting continuous time white box model for the cavity with fundamental modes down to  $3\pi/9$ -mode.

In the following we will start with analysis of signals from the cavities operated at one RF station at the European XFEL.

### (1) FFT of Cavity Signal

Figure 3 shows an example of FFT for 2 cavities at one RF station of XFEL. In this example the system is oper-

Table 1: Selected Cavity Parameters for the First Six Additional Resonant Modes Next to the  $\pi$ -mode [9].

Mode m	$8\pi/9$	$7\pi/9$	$6\pi/9$	$5\pi/9$	$4\pi/9$	$3\pi/9$
$f_m$ [kHz]	785	3053	6501	10694	15122	19237
$Q_{L,m}/Q_{L,\pi}$	0.516	0.566	0.667	0.852	1.21	2.0

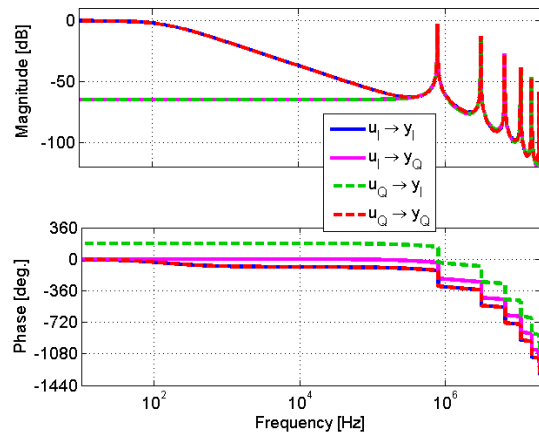


Figure 2: Continuous time cavity baseband white box model without time delay, no detuning and a loaded quality factor of  $Q_L = 4.6 \cdot 10^6$  for  $\pi$ -mode. The fundamental  $\pi$ -mode ( $f_\pi = 1.3$  GHz) is located at frequency zero.

ated in open loop, no feedback nor other advanced feedback schemes. Based on this signal it is difficult to evaluate the passband modes. The notch at around 800 kHz is given by the digitally implemented individually adjustable band-stop filter for each cavity signal. A similar characteristic has been observed in closed loop operation with correctly setup feedback controller, see MIMO controller section, and well adjusted ADC filters. Therefore, taking the FFT of a cavity probe signal does not give the full information of a cavity

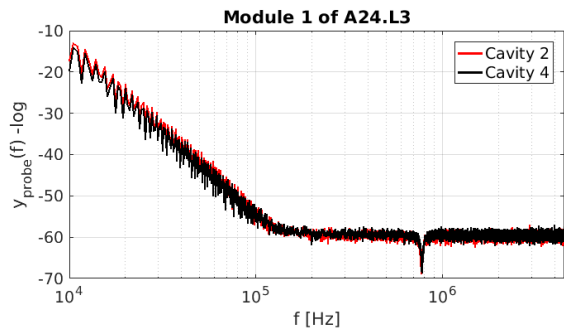


Figure 3: FFT from the 2 cavities at European XFEL operated in feedforward only.

spectrum. The excitation of narrow bandwidth resonant modes requires the excitation with their relatively precise passband frequency.

### (2) Piecewise Reconstruction of Transfer Function

By measuring the input/output characteristic response to an added excitation signal we will be able to generate a piecewise reconstruction of the plant transfer function. The cavity probe signal itself does not give a clear insight of the cavity system for the additional passband modes. We will specifically excite the system by using special signals added to the nominal drive signal. Hereby a chirp sine signal with frequency range of 500 kHz has been used. We recorded and analysed the data in 250 kHz steps from 500 kHz up to 4.5 MHz. Its amplitude is limited for safety reasons to 10.000 counts corresponding to about 10% of full scale. The recorded signals were transformed into the frequency domain and the difference between the logarithmic output and input signal corresponds to the magnitude shown in Fig. 4. The piecewise reconstruction requires several datasets for

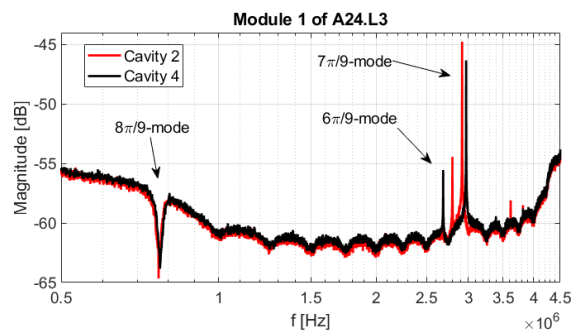


Figure 4: Piecewise reconstruction of transfer function

the excitation and the read-back signal. This is very time consuming, but necessary for improving the signal-to-noise ratio. Furthermore, the correct interaction between channels and other effects like system delay and channel couplings is a challenging reconstruction tasks. However, the frequency location of the  $8\pi/9$ -mode notch was found as it was the case for the FFT only approach. Furthermore, additional modes could be identified, i.e. at around 3 MHz the  $7\pi/9$ -mode with higher magnitude than the aliased  $6\pi/9$ -mode. This

mode is aliased from about 6.5 MHz to about 2.8 MHz for C2 and to 2.7 MHz for C4 using a sampling frequency of 4.5 MHz.

## SYSTEM IDENTIFICATION

The systematic system modelling started with signal processing and an implementation using black box modelling in 2006, [6]. This has been extended to grey box modelling approach using symmetric and non-symmetric models, [7]. The developed and used system identification is divided into several steps. First the system is excited using special signals to the plant input, i.e. the drive signal to the vector modulator in I/Q coordinates. The output signals are taken and pre-processed. Based on the I/O data-set the system model is estimated using a black- or a grey-box model. The estimated model and dataset taken can be saved for later use or off-line analysis.

The identification is implemented as an open loop characterization. The system characterization as small signal model requires the operation around the nominal operating point. Any deviation in amplitude and phase can lead to an imperfection in modelling procedure if non-linear effects (klystron, pre-amplifier, etc) dominate the system. This can be compensated by adjusting the scaling and rotation factor of the drive signal for feed-forward operation. Additional automation influencing the plant characteristic during the system modelling need to be switched off. The extraction of the system model from closed loop operation requires the precise knowledge of the feedback controller and other effects which may compensate the excitation signal, e.g. learning schemes. Following additional prerequisite must be fulfilled:

- Enable the feedforward (FF) operation
- Enable a table where the excitation signal can be applied
- Disable additional adaptations of the drive signal
- Open all feedback loops (prop. FB, MIMO, ILC)

The system identification will stop if any of these features are active and prompt the user to disable the undesired functionalities. An example for pseudo random binary (PRB) signal used to estimate the low-frequency characteristic and system delay is shown on the right plot of Fig. 1. Once the low-frequency behaviour is estimated, currently one high frequency passband mode can be added e.g. by using chirp sine excitation signals with given frequency spread. Finally, the model can be validated.

The estimated transfer function of cavity C2 including the entire high power chain is shown in Fig. 5. In this example the "ADVANCED SYSTEM SETUP TOOL" input channel has been changed to analyse single cavity signal (instead of default vector-sum). The signal delay was found to be 21 samples, i.e.  $2.3 \mu s$  from FPGA drive signal to detection of cavity probe signal for the about 9 MHz signal processing frequency. The low frequency estimation uses an independent, uncorrelated, PRB signal for the I and Q channels. An

Content from this work may be used under the terms of the CC BY 3.0 licence (© 2019). Any distribution of this work must maintain attribution to the author(s), title of the work, publisher, and DOI.

excitation using chirp sine signal with 500 kHz frequency range is then applied around the expected resonant mode at 3 MHz.

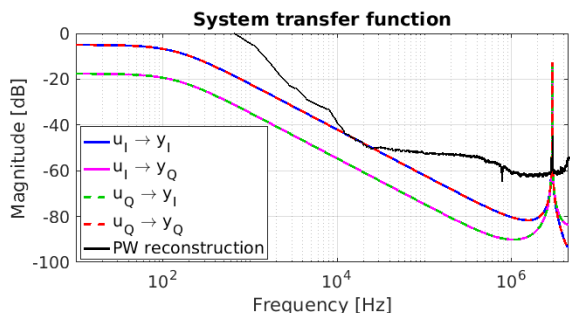


Figure 5: Grey box model identification with low-pass characteristic and  $7\pi/9$ -mode modelling for C2.M1.A24.L3. The magnitude plot using piecewise (PW) reconstruction have been added for completeness.

### Discussion

The comparison of both transfer functions in Fig. 5 shows a smaller magnitude of the  $7\pi/9$ -mode for the piecewise reconstruction, whereas the magnitude of the  $7\pi/9$ -mode for the transfer function is much larger. This is because the piecewise reconstruction requires long excitation time to build up a steady state behavior for the additional passband modes. Their bandwidth is similar to the bandwidth of the  $\pi$ -mode, see Table 1. This needs to be considered when taking the piecewise reconstruction into account. Therefore it is beneficial to use the system identification for cavities with low bandwidth as operated for FLASH, European XFEL and other facilities. The validation in time of the  $7\pi/9$ -mode is shown in Fig. 6 and shows good agreement between the simulation and the measurement.

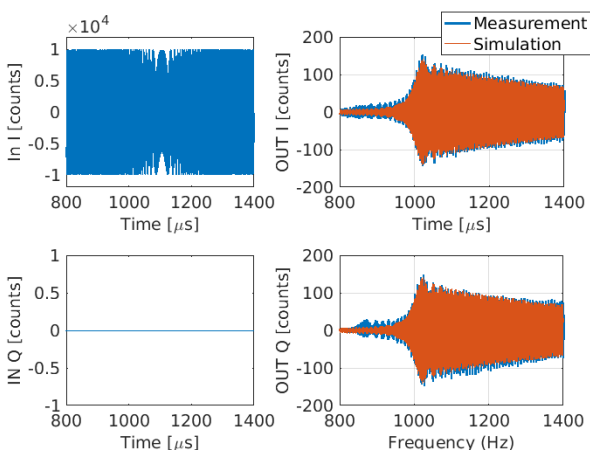


Figure 6: Grey box model simulation and measurement for  $7\pi/9$ -mode.

## MIMO CONTROLLER DESIGN

The MIMO feedback controller design relies on the system model identified before. The purpose of the SRF feedback controller design is to notch a passband mode and to decouple the closed loop system, i.e. the system under feedback regulation, [7]. For this example we will focus on vector-sum regulation at the XFEL RF station A24. The MIMO controller on the FPGA is given by  $2 \times 2$  transfer matrix, each hosting a second order filter function, see [6]. A proportional gain is implemented in series with the dynamic MIMO block to overcome fixed-point constraints of the MIMO coefficients coming from the FPGA implementation.

An analytical controller is directly computed which is only notching the passband mode, see Fig. 7. One tuning knob is sufficient to further design the controller, i.e. the parameter Pole Adjustment is shifting the bandwidth of the controller transfer function to smaller frequencies by increasing their number. This often helps to reduce high frequency noise feedback into the system. The tool checks the stability of the closed loop system by the systems infinity norm, i.e. an induced signal norm, see [7]. The resulting MIMO controller is visualized in Fig. 8. This controller can be stored via the GUI and directly written to FPGA.

## LEARNING FEEDFORWARD

The learning feedforward algorithm relies on a closed loop system model from feedforward signal to the output signal, i.e. the signal to be controlled. This closed loop model is automatically generated with the current system model and the feedback controller settings. The learning feedforward algorithm behind this is based on iterative learning control (ILC) [3, 6]. One tuning knob, i.e. the learning gain, is enough for the setup which is similar to the MIMO feedback controller design, see Fig. 9. Here again a stability check is inviting the user to lower the learning gain if a certain threshold is exceeded. Writing and saving the previous and updated parameter is automatically done.

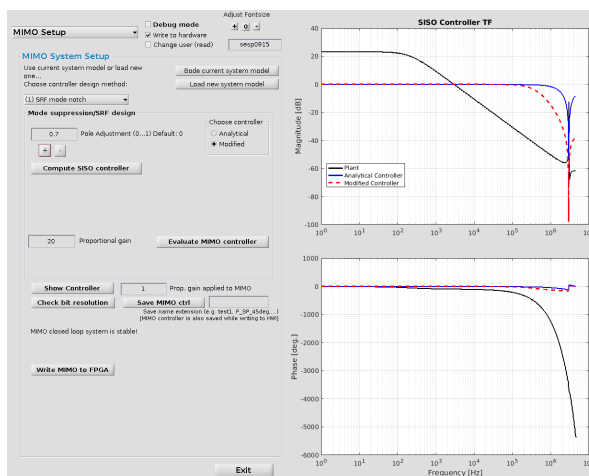


Figure 7: MIMO GUI part from Fig. 1 with replaced system identification (middle) part.

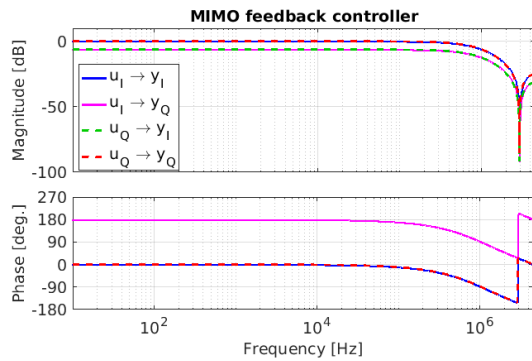


Figure 8: Example for MIMO controller.

## CONCLUSION

The systematic MIMO and LFF setup is realized via a GUI for all the SRF stations operated at DESY. The tool could be extended to be used in several facilities based on a similar LLRF system. The RF stations at FLASH and XFEL were setup using this tool. An RF regulation example at the European XFEL is given in Fig. 10. Hereby open loop, closed loop by MIMO and MIMO together with learning feedforward are compared. The open loop case shows highest variations in amplitude and phase, far beyond the specifications and outside of the standard deviation plot.

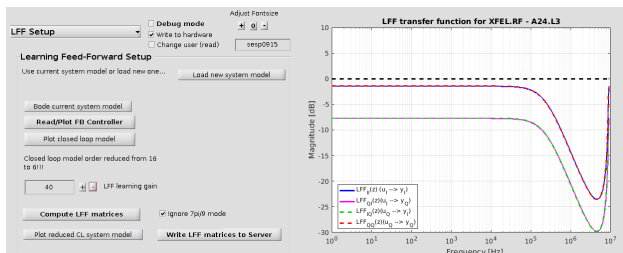


Figure 9: LFF GUI part from Fig. 1 with replaced middle part.

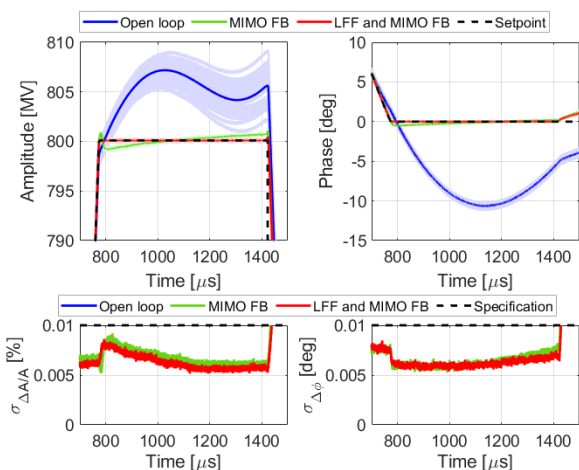


Figure 10: Example for systematic RF field controller setup at XFEL using model-based MIMO feedback controller and learning feedforward adaptation

Closing the feedback loop brings the regulation close to the desired setpoint trajectory with mean-free standard deviation within the specifications, but with an error between setpoint and vector-sum. This remaining repetitive error is reduced using the adaptive adjustment of the drive signal by learning feedforward. The tool has also been tested for CW setup at the cryomodule test bench at DESY (CMTB) and at the ELBE accelerator (HZDR) using model-based PI(D) regulation scheme.

## ACKNOWLEDGEMENT

We acknowledge the FLASH and European XFEL operation teams for giving us the opportunity of developing and testing the setup tools during regular machine operation. Furthermore, we would like to thank the ELBE LLRF team at HZDR for allowing us to do system characterization and testing various feedback controllers of their SRF cavities operated in CW-mode. This work was supported by the Helmholtz Association within the topic Accelerator Research and Development (ARD) of the Matter and Technologies (MT) Program.

## REFERENCES

- [1] M. Altarelli *et al.*, “XFEL, the European X-ray free-electron laser: Technical design report”, DESY XFEL Project Group, 2006.
- [2] MTCA.4, “MTCA.4 for Industry and Research,”, 2013. <http://mtca.desy.de>
- [3] S. Kirchhoff, C. Schmidt, G. Lichtenberg, H. Werner, “An iterative learning algorithm for control of an accelerator based Free Electron Laser,” in *Proceedings of the 47th IEEE Conference on Decision and Control*, 2008, pp. 3032–3037.
- [4] C. Schmidt, G. Lichtenberg, W. Koprek, W. Jałmużna, H. Werner, S. Simrock, “Parameter estimation and tuning of a multivariable RF controller with FPGA technique for the Free Electron Laser FLASH,” in *Proceedings of the American Control Conference*, 2008, pp. 2516–2521.
- [5] H. Langkowski, C. Schmidt, G. Lichtenberg, H. Werner, “An Iterative Learning Control Approach combined with a Multivariable RF Controller for the Free Electron Laser FLASH,” in *Proceedings of the European Control Conference*, 2009, pp. 442–447.
- [6] C. Schmidt, “RF System Modeling and Controller Design for the European XFEL,” Ph.D. thesis, Hamburg University of Technology, Hamburg, Germany, 2010.
- [7] Sven Pfeiffer, “Symmetric Grey Box Identification and Distributed Beam-Based Controller Design for Free-Electron Lasers,” Ph.D. thesis, Hamburg University of Technology, Hamburg, Germany, 2014.
- [8] T. Schilcher, “Vector sum control of pulsed accelerating fields in lorentz force detuned superconducting cavities”, Hamburg University, 1998.
- [9] E. Vogel, “High gain proportional rf control stability at TESLA cavities,” *Physical Review Special Topics - Accelerators and Beams*, vol. 10, p. 052001, 2007.